



Full Length Article

Effect of gold nanoparticles shape and size on the photophysicochemical behaviour of symmetric and asymmetric zinc phthalocyanines

Edith Dube, Tebello Nyokong*

Center for Nanotechnology Innovation, Department of Chemistry, Rhodes University, Grahamstown 6140, South Africa

ARTICLE INFO

Keywords:

Gold nanotriangles
Nanospheres
Triplet quantum yield
Zinc phthalocyanines
Asymmetry

ABSTRACT

Glutathione (GSH) capped Au nanotriangles (AuNTs–GSH) and nanospheres (AuNSs–GSH) are covalently linked to symmetric Zn phthalocyanine (ZnPc) substituted with phenoxy propanoic acid substituents only (complex 1) and two asymmetric ZnPc, each containing one phenoxy propanoic acid and three benzothiazole phenoxy moieties (complex 2), and one phenoxy propanoic acid and no other ligands (complex 3). The photophysicochemical behaviour of Pc complexes and their conjugates were studied. All conjugates displayed improved triplet and singlet oxygen quantum yields with decreases in fluorescence quantum yields compared to their respective Pc complexes. The conjugates of asymmetric complexes 2 and 3, afforded much higher triplet and singlet oxygen quantum yields compared to the symmetric complex 1, and could serve as good candidates for photodynamic therapy.

1. Introduction

Metallophthalocyanines (MPcs) are dyes that have found use as photosensitisers (PS) in applications such as photodynamic therapy (PDT) [1–3], photodynamic antimicrobial chemotherapy (PACT) [4–6], photodegradation of pollutants [7] and nonlinear optics [8]. The presence of heavy atoms in the central cavity of Pcs promotes intersystem crossing to a triplet state [9]. The triplet state reacts with the ground state molecular oxygen via energy transfer to form singlet oxygen and other reactive oxygen species that can destroy cancer cells and pathogenic microbes. The efficiency of singlet oxygen generation of a PS is important in applications such as in PACT, PDT and photodegradation of pollutants [10].

Selective accumulation of the PS to cancerous cells is paramount in PDT applications [11,12], and as a result, studies on the use of nanocarriers are on the increase. Gold nanoparticles have been linked to MPcs as nanocarriers for improved targeting through the enhanced permeability and retention (EPR) effect [13]. The attractiveness of gold as a nanocarrier emanates from its biocompatibility, inertness and non-toxicity within biological systems [14]. Its ability to improve the photophysical and photochemical properties of MPcs through the heavy atom effect is an added advantage.

This work reports on the covalent linkage of symmetric (complex 1) and asymmetric (complexes 2 and 3) zinc phthalocyanines to glutathione functionalized gold nanotriangles (AuNTs–GSH) and

nanospheres (AuNSs–GSH). Zinc phthalocyanines are employed in this work since they are known to possess high triplet and singlet oxygen quantum yields. We then compare the photophysical behaviour of the gold conjugates of the symmetric ZnPc (with phenoxy propanoic acid substituents only, complex 1) and those of two asymmetric ZnPc, each containing one phenoxy propanoic acid and three benzothiazole phenoxy moieties for complex 2, and no other groups for complex 3. Porphyrins containing propanoic acid (such as the Uroporphyrins) have been successfully applied for PDT [2], hence the interest in Pcs containing propanoic acid substituents, additionally Pc complexes containing phenoxy propanoic acid displayed reasonably high triplet and singlet oxygen quantum yield [15,16]. The covalent linkage of gold nanotriangles to phthalocyanines is reported for the first time and this is further compared with covalent linkage of the corresponding phthalocyanines with gold nanospheres. The conjugates of phthalocyanines (Pc) with gold spheres (AuNS) have been compared with those of rods, stars and bipyramids [17], however we compare for the first time the conjugates of spheres with those of triangles. Gold nanotriangles were reported to display better cellular uptake compared to other anisotropic nanoparticles (order of cellular uptake efficiency: triangles > rods > stars [18]), while on the other hand a simulation model of gold nanoparticles demonstrated the highest uptake of nanospheres compared to rods, cubes and disks [19]. An efficient cellular uptake is good for applications in photodynamic therapy. For the covalent linkage, the carboxylic acid of the Pcs was linked to the amino

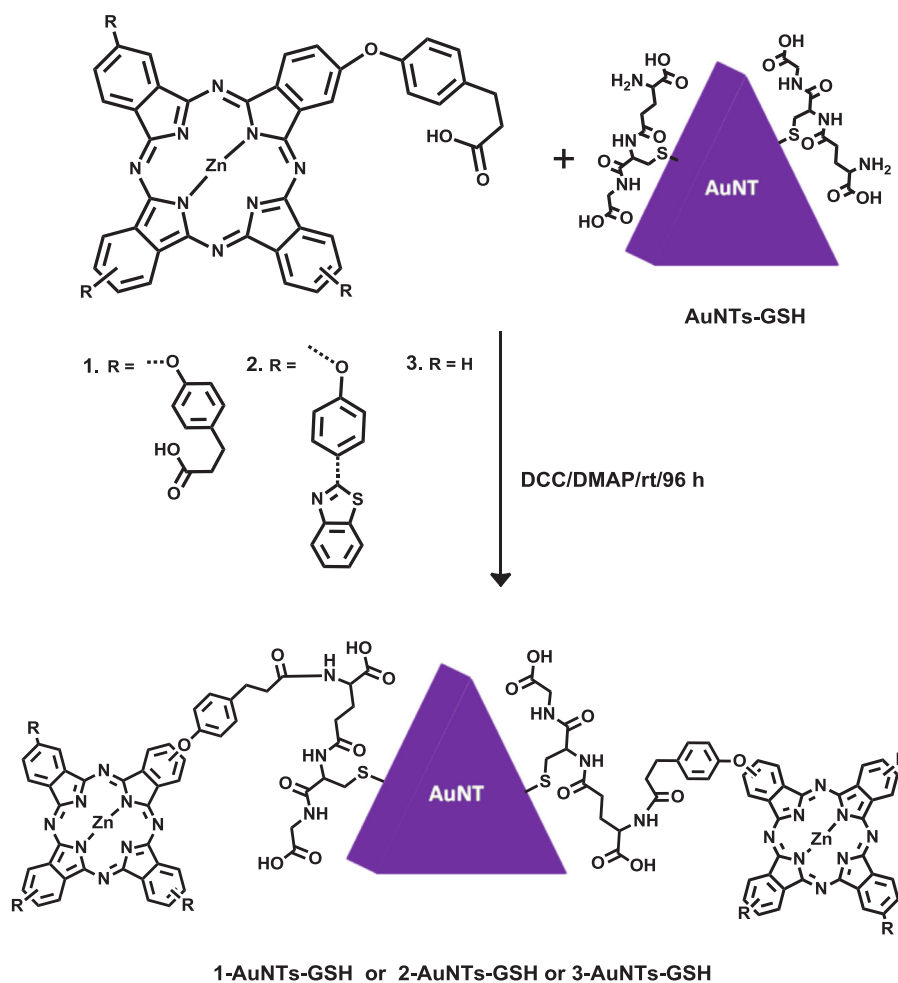
* Corresponding author.

E-mail address: t.nyokong@ru.ac.za (T. Nyokong).<https://doi.org/10.1016/j.jlumin.2018.09.063>

Received 19 July 2018; Received in revised form 10 September 2018; Accepted 28 September 2018

Available online 01 October 2018

0022-2313/ © 2018 Elsevier B.V. All rights reserved.



Scheme 1. Illustration of Synthetic pathways for 1-AuNTs-GSH, 2-AuNTs-GSH and 3-AuNTs.

group of the glutathione functionalized nanoparticles via an amide bond.

2. Experimental

2.1. Materials

Ultra-pure water (from a Milli-Q Water System, Millipore Corp, Bedford, MA, USA), 1,3-diphenylisobenzofuran (DPBF), N,N'-dicyclohexylcarbodiimide (DCC), 4-(dimethylamino)pyridine (DMAP), anthracene-9,10-bis-methylmalonate (ADMA) and zinc phthalocyanine (ZnPc) were purchased from Sigma–Aldrich. Absolute ethanol and methanol were purchased from SAARCHEM. Dimethyl sulphoxide (DMSO) and N,N-dimethyl formamide (DMF) were purchased from Merck. All other reagents and solvents were obtained from commercial suppliers and used as received. AlPcSmix (mixture of sulfonated derivatives) was used as a standard for singlet oxygen quantum yields and was synthesized according to literature methods [20]. The syntheses of complexes **1** [15], **2** [16], and **3** [15], and of glutathione (GSH) functionalized gold nanospheres (AuNSs) [21] and gold nanotriangles (AuNTs) [22], have been reported.

2.2. Equipment

Ground state electronic absorption was measured using a Shimadzu UV-2550 spectrophotometer. Infrared spectra were acquired on a Bruker ALPHA FT-IR spectrometer with universal attenuated total reflectance (ATR) sampling accessory. Fluorescence excitation and

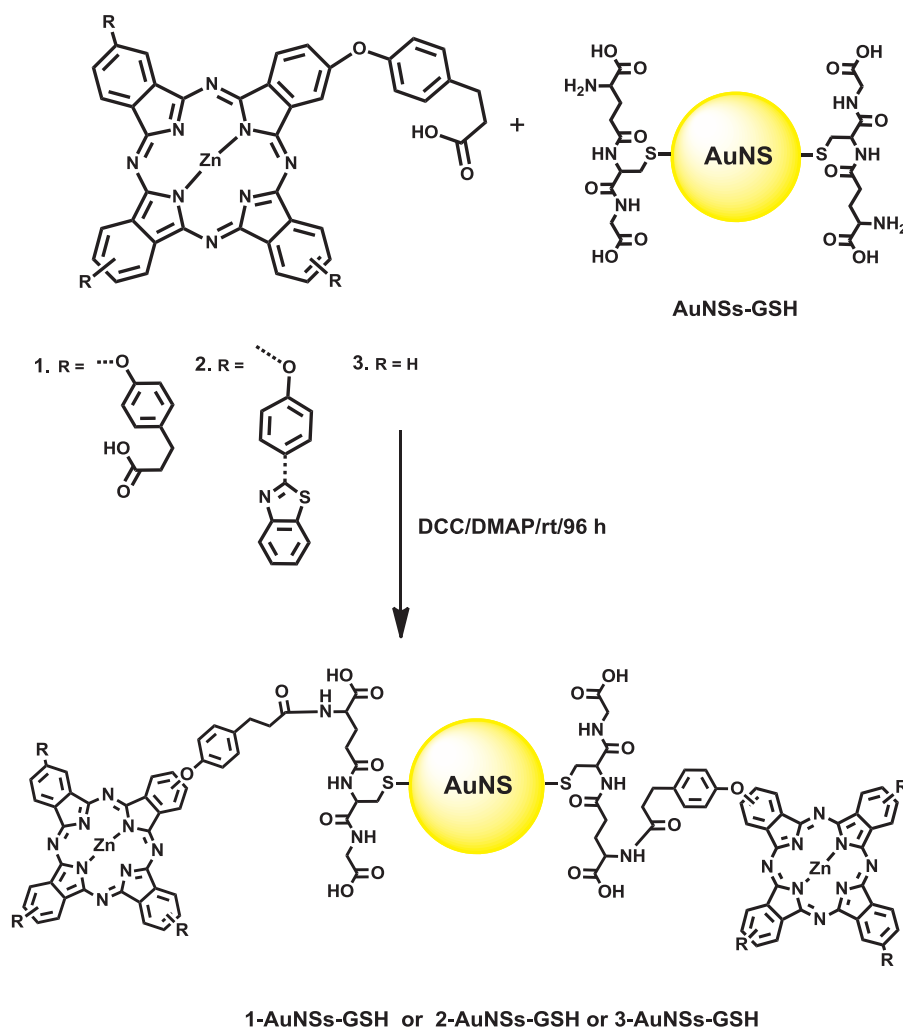
emission spectra were measured on a Varian Eclipse spectrofluorometer using a 360–1100 nm filter. Excitation spectra were recorded using the Q-band of the emission spectra.

Fluorescence lifetimes were measured using a time correlated single photon counting setup (TCSPC) (FluoTime 300, Picoquant GmbH) with a diode laser (LDH-P-670, Picoquant GmbH, 20 MHz repetition rate, 44 ps pulse width) [15,16].

Triplet quantum yields were determined using a laser flash photolysis system consisting of a LP980 spectrometer with a PMT-LP detector and an ICCD camera (Andor DH320T-25F03). The signal from a PMT detector was recorded on a Tektronix TDS3012C digital storage oscilloscope. The excitation pulses were produced using a tunable laser system consisting of an Nd: YAG laser (355 nm, 135 mJ/4–6 ns) pumping an optical parametric oscillator (OPO, 30 mJ/3–5 ns) with a wavelength range of 420–2300 nm (NT-342B, Ekspla).

Irradiation for singlet oxygen quantum yield determinations were performed using a general electric quartz lamp (300 W) as described in the literature [23]. Light intensity was measured with a POWER MAX 5100 (Molelectron detector incorporated) power meter and was found to be 4.3×10^{15} photons $\text{cm}^{-2} \text{s}^{-1}$.

X-ray powder diffraction patterns were recorded using a Cu K radiation (1.5405 Å, nickel filter), on a Bruker D8 Discover equipped with a proportional counter and the data was processed using the Eva (evaluation curve fitting) software. Transmission electron microscope (TEM), ZEISS LIBRA[®] model 120 operated at 90 kV was used for the assessment of morphologies of the nanoparticles (NPs) and their conjugates. Elemental compositions of the NPs and the conjugates were qualitatively determined using energy dispersive X-ray spectroscopy



Scheme 2. Illustration of Synthetic pathways for 1-AuNSs-GSH, 2-AuNSs-GSH, and 3-AuNSs-GSH.

(EDX), INCA PENTA FET coupled to the VAGA TESCAM operated at 20 kV accelerating voltage.

2.3. Linkage of complexes 1 and 2 to AuNTs-GSH (Scheme 1) and AuNSs-GSH (Scheme 2)

AuNTs [22] and AuNSs [21] were synthesized and functionalized with glutathione as reported in the literature. The Pc complexes were covalently linked to the NPs to form conjugates as follows: complex 1 (0.021 g, 0.017 mmol), complex 2 (0.023 g, 0.016 mmol), and 3 (0.012 g, 0.016 mmol) were separately dissolved in 2 mL of dry DMF. The coupling agents, DCC (0.01 g, 0.049 mmol) and DMAP (0.005 g, 0.042 mmol) were added to activate the carboxylic acid group of the Pc complexes to allow for covalent linkage to NPs via amide bond formation. The reaction mixtures were stirred for 48 h at room temperature after which 0.05 g of AuNTs-GSH was added and the reaction mixture was further stirred for 48 h. The same protocol was employed for AuNSs-GSH. The conjugates (1-AuNTs-GSH, 1-AuNSs-GSH, 2-AuNTs-GSH, 2-AuNSs-GSH, 3-AuNTs-GSH, and 3-AuNSs-GSH) were precipitated out with methanol and centrifuged. The precipitates were purified by washing with ethanol (with centrifuging) and allowed to dry in the fume hood.

2.4. Photophysical studies

Fluorescence (Φ_F) and triplet (Φ_T) quantum yields of Pc complexes and the conjugates were determined in DMSO using comparative methods described before in literature [24,25]. Unsubstituted ZnPc in DMSO was used as a standard with $\Phi_F = 0.20$ [24] and $\Phi_T = 0.65$ [26]. The solutions for triplet state studies were de-aerated with argon for 15 min before measurements.

Singlet oxygen quantum yield (Φ_{Δ}) values were determined under ambient conditions using DPBF as a singlet oxygen quencher in DMSO (and ADMA in water) and equations described before [27,28]. ZnPc in DMSO was used as a standard ($\Phi_{\Delta(\text{Std})} = 0.67$ in DMSO) [27]. AIPcSmix was employed as a standard in aqueous media ($\Phi_{\Delta(\text{Std})} = 0.42$ [25]). The absorbances of DPBF or ADMA were spectroscopically monitored at 417 nm or 380 nm, respectively, at predetermined time intervals.

3. Results and discussion

3.1. Characterization of NPs and conjugates

Schemes 1 and 2 show the covalent linkage of Pc complexes to AuNTs-GSH and AuNSs-GSH respectively via an amide bond between the carboxylic acid of the propanoic acid substituents and the amino group of glutathione in glutathione functionalized gold nanoparticles. Complex 2 also has a benzothiazole substituent which contains sulphur, known for its affinity for gold. It should however be noted that the

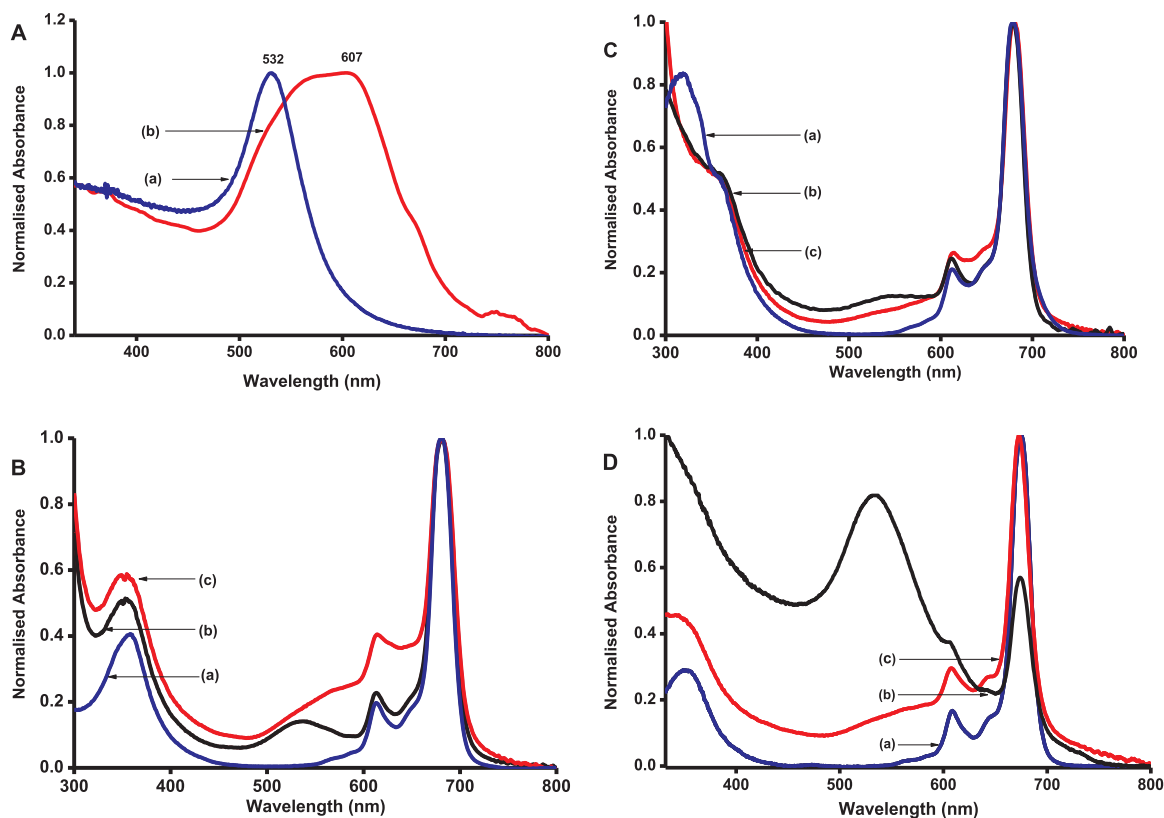


Fig. 1. UV-vis absorption of (A) AuNSs-GSH (a), AuNTs-GSH (b), (B) complex 1 (a), 1-AuNSs-GSH (b), 1-AuNTs-GSH (c), (C) complex 2 (a), 2-AuNSs-GSH (b), 2-AuNTs-GSH (c), (D) complex 3 (a), 3-AuNSs-GSH (b), 3-AuNTs-GSH (c) in DMSO.

Table 1

Photophysicochemical parameters of complexes 1, 2 and their conjugates in DMSO.

Samples	Size (TEM) (nm) ^a	Pc loading ($\mu\text{g}/\text{mg}$)	$\lambda_{\text{abs}}(\text{nm})$	$\Phi_{\text{F}} (\pm 0.01)$	$\tau_{\text{F}}(\text{ns}) (\pm 0.01)$	$\Phi_{\text{T}} (\pm 0.01)$ (DMSO)	$\tau_{\text{T}}(\mu\text{s}) (\pm 1.00)$	$\Phi_{\Delta} (\pm 0.01)$ ^b
^c 1	–	–	680	0.19	3.36	0.54	264	0.47 (0.07)
1-AuNTs-GSH	34.9 (33.2)	22	680	0.13	3.05	0.68	244	0.59 (0.14)
^c 1-AuNSs-GSH	14.9 (13.6)	27	679	0.03	2.87	0.70	305	0.58 (0.15)
^c 2	–	–	680	0.15	2.86	0.73	238	0.69 (0.15)
2-AuNTs-GSH	37.1 (33.2)	30	681	0.08	2.30	0.83	229	0.75 (0.20)
2-AuNSs-GSH	19.8 (17.7)	37	679	0.06	2.24	0.90	216	0.79 (0.22)
^c 3	–	–	675	0.18	3.21	0.73	233	0.55 (0.12)
3-AuNTs-GSH	36.9 (33.2)	16	673	0.06	3.09	0.80	247	0.69 (0.17)
^c 3-AuNSs-GSH	13.8 (13.6)	20	674	0.02	2.98	0.87	262	0.72 (0.23)

^a Sizes as edge length for AuNTs-GSH and diameter for AuNSs-GSH; numbers in brackets are the sizes in nm for AuNTs-GSH or, AuNSs-GSH alone.

^b numbers in brackets are the values in water and for complexes alone (1, 2 and 3) the values are in water containing 0.5% DMSO.

^c Literature values for 1 and 3 [15], for 2 [16].

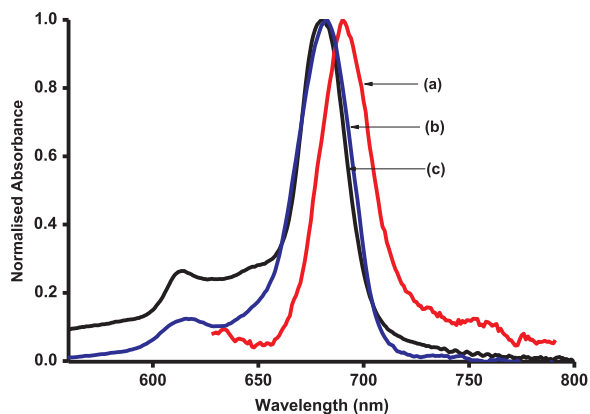


Fig. 2. Emission (a), excitation (b) and absorption (c) spectra of 2-AuNTs-GSH (excitation = 609 nm, solvent = DMSO).

presence of the capping agent, GSH, reduces the Au-S interactions. At the same time, the activated carboxylic acid moieties of 2 are expected to interact with the NH_2 group of GSH faster than the possible interaction of sulphur in benzothiazole with Au in glutathione functionalized gold nanoparticles.

Though the Pc complexes alone are not water soluble, the presence of glutathione in nanoparticles makes the conjugates readily soluble in water, which is important for practical applications. However, singlet oxygen determinations of the Pc complexes alone in water were carried out using 0.5% DMSO in water.

3.1.1. Electronic Absorption and emission spectra of complexes and their conjugates

The surface plasmon peaks of AuNTs-GSH and AuNSs-GSH (Fig. 1) were observed at 607 nm (dipole peak) and 532 nm, respectively. The AuNTs-GSH also displayed a shoulder peak at 600 nm, and this could be attributed to the presence of another size (smaller) of nanotriangles.

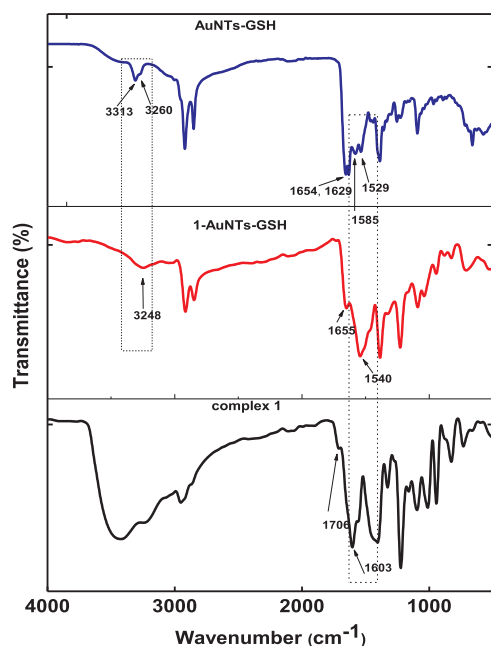


Fig. 3. FTIR spectra of AuNTs-GSH, 1-AuNTs-GSH and complex 1.

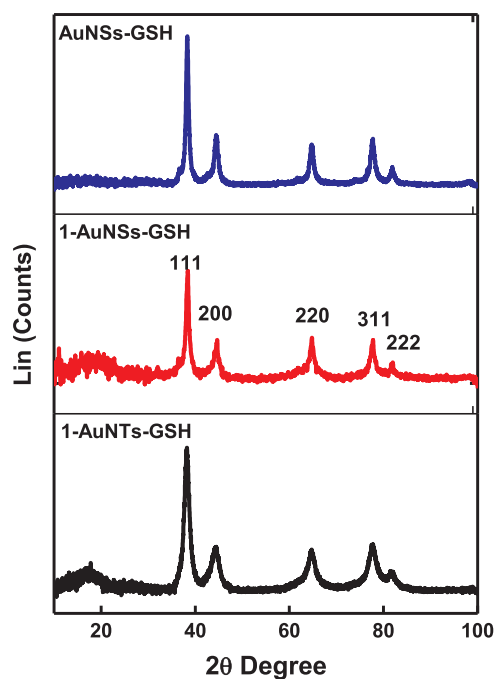


Fig. 4. XRD diffractograms for AuNSs-GSH, 1-AuNSs-GSH and 1-AuNTs-GSH.

The electronic absorption spectra of **1**, **2** and **3** and their conjugates with both AuNTs-GSH and AuNSs-GSH are shown in Fig. 1. The Q bands for **1** and **2** are red shifted compared to **3**, Table 1. For complex **2** the red-shifting is due to the presence of S and N atoms which are known to red-shift the Q band [23]. The Pc complexes alone display minimum to no absorption between 400 nm and 600 nm; however, upon linkage to AuNPs there was enhancement of absorption especially between the 400–650 nm regions, confirming successful linkage. The linkage of AuNSs-GSH to complexes **1** and **2** red shifted the SPR peak from 532 nm to 535 nm (Fig. 1B(b)) and 549 nm (Fig. 1C(b)), for 1-AuNSs-GSH and 2-AuNSs-GSH, respectively, while 3-AuNSs-GSH was blue shifted at 530 nm (Fig. 1D(c)). The red shifting is usually associated with an increase in size of the nanoparticles after linkage to Pc

complexes [21], however it should be noted that aggregation can also lead to an increase in size. The SPR peaks for 1-AuNTs-GSH, 2-AuNTs-GSH, and 3-AuNTs-GSH overlapped with the vibronic band of the phthalocyanines, hence the peaks are not clear. In water (Fig S1B, ESI[†]), the conjugates display broad bands due to aggregation typical of Pcs in aqueous solution [29] resulting from π - π electron interaction of the aromatic rings of Pcs.

The loading of complexes **1** to **3** onto the nanoparticles was investigated following literature methods [30]. This involves comparing the Q band absorbance intensity of the Pc in the conjugate with that of the initial Pc before the conjugation. The loadings of Pc onto nanoparticles are listed in Table 1. There is less loading for the AuNTs compared to AuNSs. Nanotriangles (also termed nanoplates) have a tendency to stack on each other face-to-face or edge to edge [31], and this could be the reason for less loading compared to nanospheres.

The emission, excitation and absorption spectra of 2-AuNTs-GSH (as an example) are shown in Fig. 2. The emission spectra were mirror images of the excitation spectra. The ground state electronic absorption and excitation spectra of Pcs are usually similar, however slight differences are observed in the conjugates probably due to the absorbance by the AuNPs.

3.1.2. FTIR spectra

The FTIR spectra (Fig. 3, using AuNTs-GSH, 1-AuNTs-GSH and complex **1**, as examples) were employed to prove amide bond formation between the Pc complexes and the NPs. The FTIR spectrum of AuNTs-GSH exhibited characteristic primary carboamide double peaks at 1529–1585 cm^{-1} and 3260–3313 cm^{-1} which changed to single (secondary carboamide) peaks at 1540 cm^{-1} and 3248 cm^{-1} , respectively on linkage of AuNTs-GSH to complex **1**, confirming the formation of an amide bond between glutathione functionalized NPs and the Pc complexes. Also observed was the disappearance of peaks at 1706 cm^{-1} and 1603 cm^{-1} in complex **1** and 1629 cm^{-1} in AuNTs-GSH. Shifts and changes in the IR bands confirm structural change [32]. An amide peak was observed at 1655 cm^{-1} after conjugation; however, it should be noted that GSH alone has amide bonds shown by peaks at 1654 cm^{-1} and 1629 cm^{-1} in AuNTs-GSH.

The same trend was also observed for the conjugates 1-AuNSs-GSH, 2-AuNSs-GSH, 2-AuNTs-GSH, 3-AuNSs-GSH and 3-AuNTs-GSH,

3.1.3. XRD studies

Fig. 4 shows the powder XRD patterns of AuNSs-GSH, 1-AuNSs-GSH and 1-AuNTs-GSH, used as examples. The XRD diffraction patterns are characterized by well-defined crystalline peaks at $2\theta = 38.1, 43.9, 64.5, 77.4$ and 81.0° , assigned to the 111, 200, 220, 311 and 222 planes, corresponding to the face centered-cubic structures of metallic gold [33], confirming its presence. Broad peaks between $2\theta = 15$ – 23° , characteristic of the amorphous nature of phthalocyanines [34] were observed, which provides evidence for the presence of the phthalocyanines in the conjugates.

3.1.4. TEM

The TEM micrographs of AuNTs-GSH, 1-AuNTs-GSH are shown in Fig. 5A,C, respectively, and those of AuNSs-GSH, 1-AuNSs-GSH in Fig. 5B,D, respectively. The AuNTs-GSH and AuNSs-GSH are mostly monodispersed when alone and show aggregation after linkage to Pcs. Aggregation is common in the Pc-NP conjugates, and is mostly attributed to π - π stacking that can occur between the Pcs on adjacent NPs. Pcs are known for their π - π stacking tendency to form H aggregates [29]. The average sizes of the NPs (edge lengths for AuNTs-GSH and diameter for AuNSs-GSH) and their conjugates are displayed in Table 1. Increase in size was observed in all conjugates due to aggregation as discussed above.

3.1.5. EDX

The elemental compositions of the nanoparticles, Pcs and

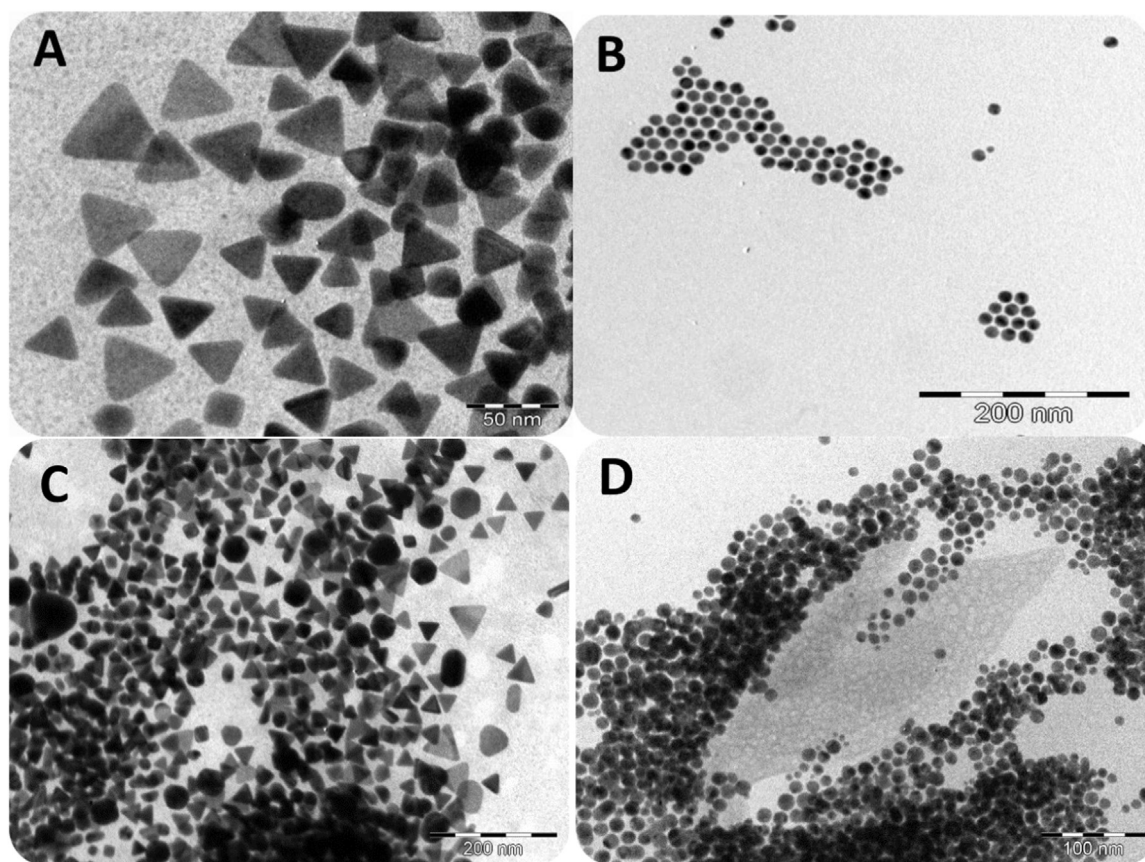


Fig. 5. Representative TEM micrographs for AuNTs-GSH (A), AuNSs-GSH (B), 1-AuNTs-GSH (C), and 1-AuNSs-GSH (D).

conjugates were qualitatively determined using an energy dispersive X-ray spectrometer (EDX) and Fig. 6 shows the spectra for AuNTs-GSH, complex 2 and 2-AuNTs-GSH as examples. The EDX spectra for AuNTs-GSH showed the presence of C, N, O, S and Au, while complex 2 showed C, N, O, S and Zn as expected for this Pc. The spectrum for 2-AuNTs-GSH displayed C, N, O, S, Au and Zn, confirming the presence of both the nanoparticle and the phthalocyanine.

3.2. Photophysicochemical parameters

The fluorescence quantum yields (Φ_F) and lifetimes (τ_F), triplet quantum yields (Φ_T) and lifetimes (τ_T), and singlet oxygen quantum yields (Φ_Δ) of complexes 1, 2, and 3 alone, and their conjugates using DMSO (and in water in brackets) are as displayed in Table 1.

3.2.1. Fluorescence quantum yields (Φ_F) and lifetimes (τ_F)

When comparing Pcs alone, complexes 1 and 3 containing no benzothiazole phenoxy groups, have about the same Φ_F values which is higher than for 2, suggesting quenching by benzothiazole substituent for the latter. On covalent linkage to AuNSs-GSH and AuNTs-GSH, all Pcs exhibited reduced Φ_F (Table 1), as expected due to the heavy atom effect of gold, which promotes intersystem crossing to the triplet state thus reducing fluorescence. The AuNSs-GSH conjugates showed lower Φ_F than their corresponding AuNTs-GSH conjugates, probably due to the higher number of Pcs loaded on the former compared to the latter. The higher number of Pcs could lead to aggregation, resulting in quenching of fluorescence.

Fluorescence behaviour of dyes in the presence of nanoparticles has been shown to be affected by the size of the nanoparticles [35], with the smaller NPs exhibiting a greater quenching effect. This is observed in this work where 1-AuNSs-GSH and 3-AuNSs-GSH, with relatively smaller size of the NSs compared to 2-AuNSs-GSH, have smaller Φ_F

values, Table 1. This also applies when comparing the larger size of AuNTs-GSH (33.2 nm-edge length) with the smaller AuNSs-GSH (17.7/13.6 nm diameter), where there is more quenching of Φ_F for complexes in the presence of the latter.

The conjugates displayed a bi-exponential decay, hence existence of two lifetimes (Fig. 7, using 3-AuNTs-GSH as example), possibly due to different orientations of the phthalocyanines on the NPs [36]. The average lifetimes for the conjugates are presented in Table 1. The fluorescence lifetimes decreased with the decrease in Φ_F since the two have a direct relationship.

3.2.2. Triplet quantum yields (Φ_T) and lifetimes (τ_T)

The Φ_T greatly influences the singlet oxygen production, thus high Φ_T , corresponding to low Φ_F , signal a more efficient intersystem crossing, an attractive feature for photosensitizers. The triplet decay and transient curve of the conjugate 1-AuNTs-GSH, (as an example) are shown in Fig. 8. The transient curve is characterized by a broad band between 380 and 600 nm with a peak at 500 nm, attributed to the triplet-triplet state excited absorption ($T_1 \rightarrow T_n$). The negative peaks shown around 358 nm and 681 nm are attributed to the depletion of the phthalocyanine's ground state [37]. The triplet decay curve obeyed second order kinetics, typical of MPc complexes at high concentration, due to triplet-triplet recombination [38]. Comparing Pcs alone, the asymmetrical complexes 2 and 3 show a much larger Φ_T values compared to 1. Asymmetry is known to introduce distortions [39], resulting in faster intersystem crossing to the triplet state, consequently increasing the triplet state population. The conjugates of Pcs with NPs generally displayed further increased Φ_T (Table 1) than Pc complexes alone, corresponding to the low Φ_F , due to the presence of gold, a heavy atom as explained before. AuNTs-GSH conjugates displayed lower Φ_T values than their corresponding AuNSs-GSH counterparts. The lower Φ_T of AuNTs-GSH conjugates was attributed to less loading which probably

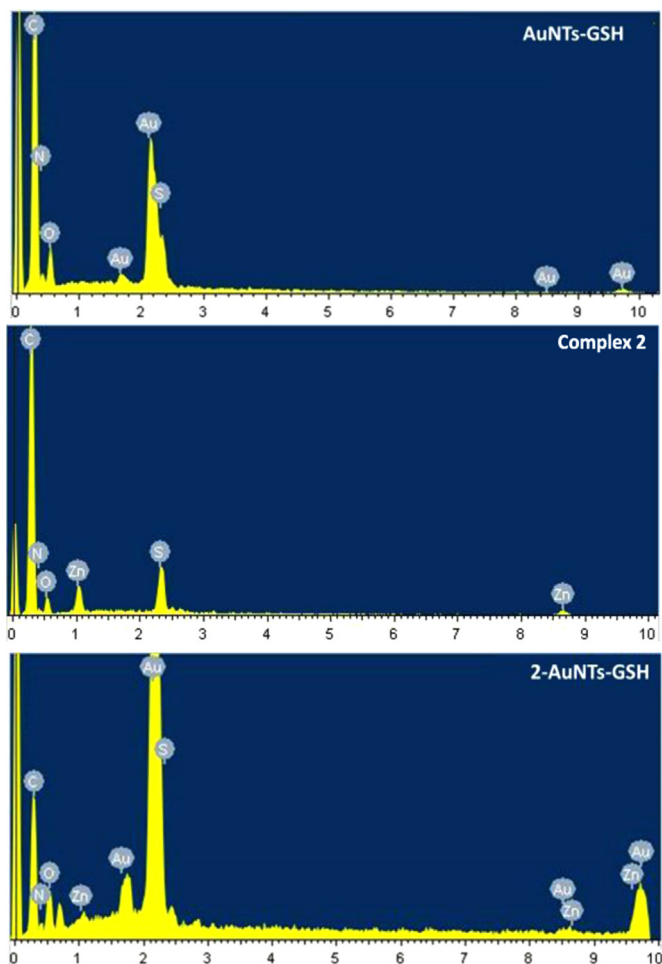


Fig. 6. EDX spectra of AuNTs-GSH, complex 2, and 2-AuNTs-GSH.

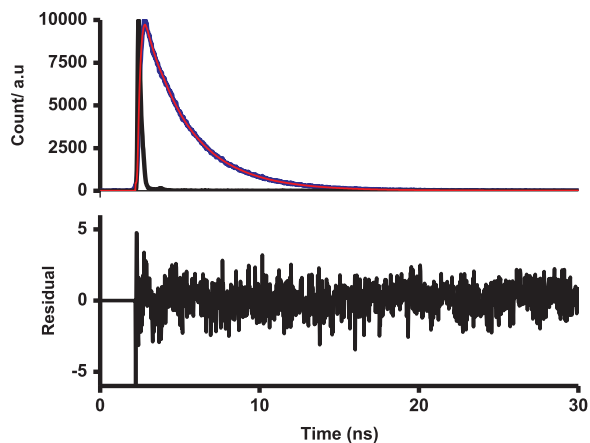


Fig. 7. Fluorescence decay (blue), χ^2 fitting (red) and IRF (black) curves for 3-AuNTs-GSH in DMSO.

was influenced by size and the tendency of nanotriangles to stack on each other as explained before. The Φ_T of the conjugates in water could not be obtained due to aggregation of phthalocyanines in water.

3.2.3. Singlet oxygen quantum yields

Singlet oxygen is produced when the PS in the excited triplet state transfers its energy to the molecular oxygen. The Φ_Δ parameter shows the efficiency of singlet oxygen production. For the determination of the singlet oxygen quantum yield (Φ_Δ), the chemical photodegradation

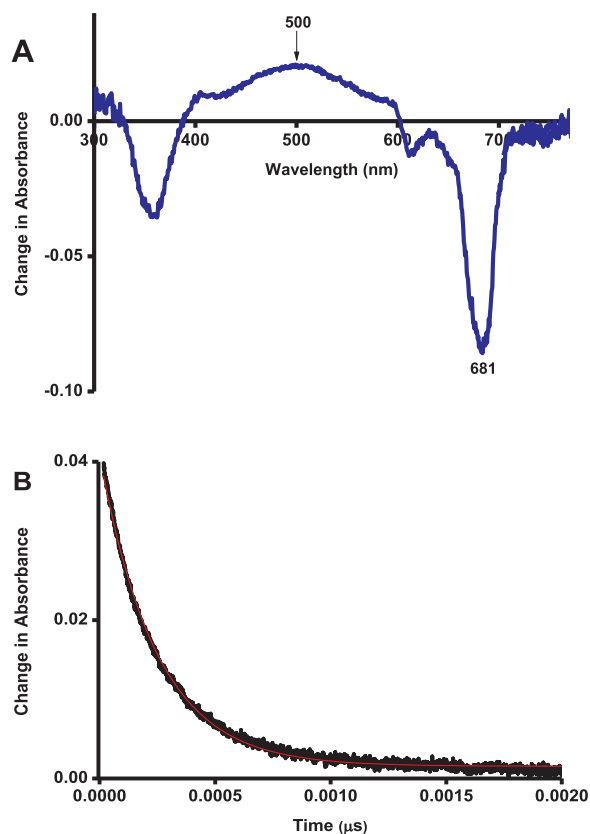


Fig. 8. (A) Transient curve and (B) triplet absorption decay curve (black) and fitting (red) for 1-AuNTs-GSH in DMSO.

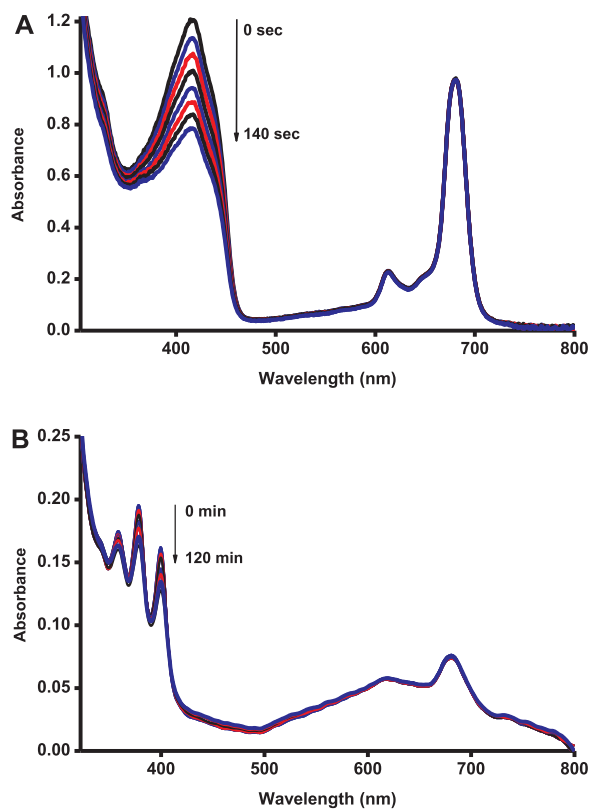


Fig. 9. Representative spectra for singlet oxygen quantum yield determination using a photochemical method. The spectra show the degradation of (A) DPBF in DMSO and (B) ADMA in water in the presence of 2-AuNTs-GSH.

of singlet oxygen quenchers (DPBF in DMSO and ADMA in aqueous media (using 2-AuNTs-GSH as an example)) were monitored over a period of time (Fig. 9). The Q-band remained unchanged, proving their stability over the irradiation period, while the DPBF and ADMA bands degraded.

The Φ_{Δ} followed the same trend observed in Φ_T since the Φ_{Δ} value is dependent on the Φ_T parameter, as previously stated. It should be noted that for studies in aqueous media, water alone was used for the conjugates since they are readily soluble as explained before, but for the Pc complexes alone which are insoluble in water, 0.5% (v/v) DMSO in water was used. Due to aggregation, the values in water are low however they still maintained the trend regardless of the slight differences in the solvent system used. PS with low Φ_{Δ} such as lutetium texaphyrin ($\Phi_{\Delta} = 0.11$) have been employed for clinical application in PDT [2], hence the Φ_{Δ} values for all conjugates shows that they may be used for PDT applications in the presence of both spherical and triangular AuNPs.

4. Conclusion

In this work, the covalent linkage of AuNTs–GSH and AuNSs–GSH to complexes 1 to 3 via an amide bond is reported. The conjugates formed were characterized using UV/vis absorption and emission spectrometer, FT-IR spectrometer, XRD, TEM and EDX. The photophysicochemical behaviour of complexes and their conjugates were studied. The linkage of complexes with nanoparticles resulted in a decrease in fluorescence quantum yields and lifetimes, which led to improved triplet and singlet quantum yields. Even though conjugates with spherical NPs displayed better properties than triangular NPs, all conjugates are ideal for PDT applications.

Acknowledgements

This work was supported by the Department of Science and Technology (DST) Innovation and National Research Foundation (NRF), South Africa through DST/NRF South African Research Chairs Initiative for Professor of Medicinal Chemistry and Nanotechnology (UID 62620) as well as Rhodes University.

Appendix A. Supplementary material

Supplementary data associated with this article can be found in the online version at <https://doi.org/10.1016/j.jlumin.2018.09.063>.

References

- [1] L.M. Moreira, F.V. dos Santos, J.P. Lyon, M. Maftoum-Costa, C. Pacheco-Soares, N.S. da Silva, Photodynamic therapy: porphyrins and phthalocyanines as photosensitizers, *Aust. J. Chem.* 61 (2008) 741–754.
- [2] R. Bonnett, In *Chemical Aspects of Photodynamic Therapy*, Gordon and Breach Science Publishers, Amsterdam, 2000.
- [3] S.B. Brown, E.A. Brown, I. Walker, The present and future role of photodynamic therapy in cancer treatment, *Lancet Oncol.* 5 (2004) 497–508.
- [4] V.N. Mantareva, I. Angelova, D. Wohrle, E. Borisovac, V. Kussovski, Metallophthalocyanines as photodynamic sensitizers for treatment of pathogenic bacteria. Uptake and photoinactivation properties, *J. Porphyr. Phthalocyanines* 17 (2013) 400–416.
- [5] D. Mondal, S. Bera, Porphyrins and phthalocyanines: promising molecules for light-triggered antibacterial nanoparticles, *Adv. Nat. Sci.: Nanosci. Nanotechnol.* 5 (2014) 033002 (12 pages).
- [6] M. Wainwright, Photodynamic antimicrobial chemotherapy (PACT), *J. Antimicrob. Chemother.* 42 (1998) 13–28.
- [7] R. Zügler, T. Nyokong, Comparative phototransformation of environmental pollutants using metallophthalocyanines supported on electrospun polymer fibers, *J. Appl. Polym. Sci.* 128 (2013) 1131–1142.
- [8] M. Hanack, T. Schneider, M. Barthel, J.S. Shirk, S.R. Flom, R.G.S. Pong, Indium phthalocyanines and naphthalocyanines for optical limiting, *Coord. Chem. Rev.* 219 (2001) 235–258.
- [9] H. Saigusa, T. Azumi, M. Sumitani, K. Yoshihara, Internal heavy atom effect on the triplet spin sublevels of the lowest triplet state of naphthalene. II. Intersystem crossing processes from the singlet excited state to the individual spin sublevels of the lowest triplet state, *J. Chem. Phys.* 72 (1980) 1713–1715.
- [10] M.C. DeRosa, R.J. Crutchley, Photosensitized singlet oxygen and its applications, *Coord. Chem. Rev.* 233–234 (2002) 351–371.
- [11] L.B. Josefsen, R.W. Boyle, Unique diagnostic and therapeutic roles of porphyrins and phthalocyanines in photodynamic therapy, *Imaging Thera. Thera.* 2 (2012) 916–966.
- [12] J. Taquet, C. Frochot, V. Manneville, M. Barberi-Heyob, Phthalocyanines covalently bound to biomolecules for a targeted photodynamic therapy, *Curr. Med. Chem.* 14 (2007) 1673–1687.
- [13] Y. Omid, J. Barar, Targeting tumor microenvironment: crossing tumor interstitial fluid by multifunctional nanomedicines, *BioImpacts: BI* 4 (2014) 55–67.
- [14] D.C. Hone, P.I. Walker, R. Evans-Gowing, S. FitzGerald, A. Beeby, I. Chambrier, M.J. Cook, D.A. Russell, Generation of cytotoxic singlet oxygen via phthalocyanine-stabilized gold nanoparticles: a potential delivery vehicle for photodynamic therapy, *Langmuir* 18 (2002) 2985–2987.
- [15] E. Dube, N. Nwaji, D.O. Oluwole, J. Mack, T. Nyokong, Investigation of photophysicochemical properties of zinc phthalocyanines conjugated to metallic nanoparticles, *J. Photochem. Photobiol. A: Chem.* 349 (2017) 148–161.
- [16] E. Dube, D.O. Oluwole, E. Prinsloo, T. Nyokong, Gold–chitosan composite with low symmetry zinc phthalocyanine for enhanced singlet oxygen generation and improved photodynamic therapy activity, *New J. Chem.* 42 (2018) 10214–10225.
- [17] T. Mthethwa, T. Nyokong, Fluorescence behavior and singlet oxygen generating abilities of aluminum phthalocyanine in the presence of anisotropic gold nanoparticles, *J. Lumin.* 157 (2015) 207–214.
- [18] X. Xie, J. Liao, X. Shao, Q. Li, Y. Lin, The Effect of shape on Cellular Uptake of Gold Nanoparticles in the forms of Stars, Rods/Triangles, *Sci. Rep.* 7 (2017) 3827.
- [19] Y. Li, M. Kroger, W.K. Liu, Shape effect in cellular uptake of PEGylated nanoparticles: comparison between sphere, rod, cube and disk, *Nanoscale* 7 (2015) 16631–16646.
- [20] M. Ambroz, A. Beeby, A.J. McRobert, M.S.C. Simpson, R.K. Svensen, D. Phillips Preparative, analytical and fluorescence spectroscopic studies of sulphonated aluminium phthalocyanine photosensitizers, *J. Photochem. Photobiol. B: Biol.* 9 (1991) 87–95.
- [21] N. Masilela, T. Nyokong, Conjugates of low-symmetry Ge, Sn and Ti carboxy phthalocyanines with glutathione capped gold nanoparticles: an investigation of photophysical behaviour, *J. Photochem. Photobiol. A: Chem.* 223 (2011) 124–131.
- [22] L. Chen, F. Ji, Y. Xu, L. He, Y. Mi, F. Bao, B. Sun, X. Zhang, Q. Zhang, High-yield seedless synthesis of triangular gold nanoplates through oxidative etching, *Nano Lett.* 14 (2014) 7201–7206.
- [23] N. Masilela, T. Nyokong, The interaction of silver nanoparticles with low symmetry cysteinyl metallophthalocyanines and their antimicrobial effect, *J. Photochem. Photobiol. A: Chem.* 255 (2013) 1–9.
- [24] A. Ogunsipe, J.Y. Chen, T. Nyokong, Photophysical and photochemical studies of zinc (II) phthalocyanine derivatives—effects of substituents and solvents, *New J. Chem.* 28 (2004) 822–827.
- [25] T. Nyokong, E. Antunes, K.M. Kadish, K.M. Smith, R. Guillard (Eds.), In *Chapter title: Photochemical and Photophysical Properties of Metallophthalocyanines: The Handbook of Porphyrin Science*, 7 World Scientific, Singapore, 2010, pp. 247–349 (chapt. 34).
- [26] T.H. Tran-Thi, C. Desforge, C. Thiec, S.J. Gaspard, Singlet–singlet and triplet–triplet intramolecular transfer processes in a covalently linked porphyrin–phthalocyanine heterodimer, *J. Phys. Chem.* 93 (1989) 1226–1233.
- [27] N.A. Kuznetsova, N.S. Gretsova, O.A. Yuzhakova, V.M. Negrinovskii, O.L. Kaliya, E.A. Luk'yanets, New reagents for determination of the quantum efficiency of singlet oxygen generation in aqueous media, *Russ. J. Gen. Chem.* 71 (2001) 36–41.
- [28] W. Spiller, H. Kliesch, D. Wohrle, S. Hackbarth, B. Roder, G. Schnurpfeil, Singlet oxygen quantum yields of different photo-sensitizers in polar solvents and micellar solutions, *J. Porphyr. Phthalocyanines* 2 (1998) 145–158.
- [29] M.J. Stillman, T. Nyokong, C.C. Leznoff, A.B.P. Lever (Eds.), *Phthalocyanines: Properties and Applications*, 1 VCH Publishers, New York, NY, 1989.
- [30] L. Li, J.F. Zhao, N. Won, H. Jin, S. Kim, J.Y. Chen, Quantum Dot - Aluminum phthalocyanine Conjugates perform photodynamic reactions to kill cancer cells via fluorescence resonance energy transfer (FRET), *Nanoscale Res. Lett.* 7 (2012) 386–393.
- [31] Y. Bae, N.H. Kim, M. Kim, K.Y. Lee, S.W. Han, Anisotropic assembly of Ag nanoparticles, *J. Am. Chem. Soc.* 130 (2008) 5432–5433.
- [32] B.C. Smith, *Infrared Spectra Interpretation: A System Approach*, CRC Press, New York, 1998.
- [33] M.H. Majles Ara, Z. Dehghani, R. Sahraei, A. Daneshfar, Z. Javadi, F. Divsar, Diffraction patterns and nonlinear optical properties of gold nanoparticles, *J. Quant. Spectrosc. Radiat. Transf.* 113 (2012) 366–372.
- [34] Prabakaran R. Prabakaran, R. Kesavamoorthy, G.L.N. Reddy, F.P. Xavier, Structural investigation of copper phthalocyanine thin films using x-ray diffraction, raman scattering and optical absorption measurements, *Phys. Status Solidi* 229 (2002) 1175–1186.
- [35] Xue, Y. Xue, L. Dai, A. Urbas, Li Quan, Size and shape-dependent fluorescence quenching of gold nanoparticles on Perylene dye, *Adv. Opt. Mater.* 1 (2013) 581–587.
- [36] C.D. Geddes, J.R. Lakowicz (Ed.), *Topics in Fluorescence Spectroscopy*, 403 Springer, New York, 2015, pp. 64–76 (2005 as cited in: M. Ledwaba et al./J. Mol. Catal. A: Chem).
- [37] Z.N. Erol, P. Atienzar, Y. Arslanoğlu, E. Hamuryudan, H. García, Synthesis and photophysical properties of phthalocyanines having calixpyrrole units, *RSC Adv.* 5 (2015) 55901.
- [38] M.G. Debacker, O. Deleplanque, B. Van Vlierberge, F.X. Sauvage, A laser photolysis study of triplet lifetimes and of triplet–triplet annihilation reactions of phthalocyanines in DMSO solutions, *Laser Chem.* 8 (1988) 1–11.
- [39] T. Fukuda, S. Homma, N. Kobayashi, Deformed phthalocyanines: synthesis and characterization of zinc phthalocyanines bearing phenyl substituents at the 1-, 4-, 8-, 11-, 15-, 18-, 22-, and/or 25-positions, *Chem. Eur. J.* 11 (2005) 5205–5216.